

# Proliferation and regeneration of the healthy human urothelium: a multi-scale simulation approach with 16 hypotheses of cell differentiation

Angelo Torelli<sup>1\*</sup>, Philipp Erben<sup>2,3</sup>, Julian Debatin<sup>1</sup>, and Markus Gumbel<sup>1,3+</sup>

<sup>1</sup>Institute for Medical Informatics, Mannheim University of Applied Sciences, 68163 Mannheim, Germany

<sup>2</sup>Clinic of Urology, Medical Faculty Mannheim at the University of Heidelberg, 68167 Mannheim, Germany

<sup>3</sup>On behalf of the BRIDGE Consortium e.V.

+m.gumbel@hs-mannheim.de

## ABSTRACT

The urothelium as a stratified epithelium of the urinary tract is a slow regenerating tissue of different layers and shares some similarities with the epidermis. Characteristics of its cell types, tissue homeostasis and regeneration are only partly understood. Precise computer-based models which investigate the cell kinetics of the urothelium from a theoretical perspective may be beneficial for the regenerative medicine field and cancer research. We have developed an agent-based computer simulation based on the Glazier-Graner-Hogeweg (GGH) approach and tested 16 hypotheses on proliferation and differentiation mechanisms of the healthy urothelial tissue in steady state and tissue regeneration. A fitness-function was introduced for the quantitative comparison of the models. Our findings indicate that two similar hypotheses with the following features describe the healthy tissue best: 1) Stem cells either divide and differentiate in a stem cell fashion or according to the population asymmetry model in epidermis, 2) Basal cells divide symmetrically and differentiate into intermediate cells depending on contact to the basal membrane, 3) Intermediate cells do not proliferate but differentiate into umbrella cells when they are in contact with the medium.

## 1 Introduction

### 1.1 Motivation

The coordination of epithelial cell proliferation, differentiation and migration is crucial for tissue homeostasis which is interrupted in case of tissue injury or during carcinogenesis. The urothelium is a stratified epithelium of the urinary tract and builds a barrier between blood and urine. It is a slow regenerating tissue with a turnover time of 3 to 6 months<sup>1-3</sup>. However, after injury there is an enormous regeneration capability of the uroepithelium within days after significant damage<sup>1</sup>.

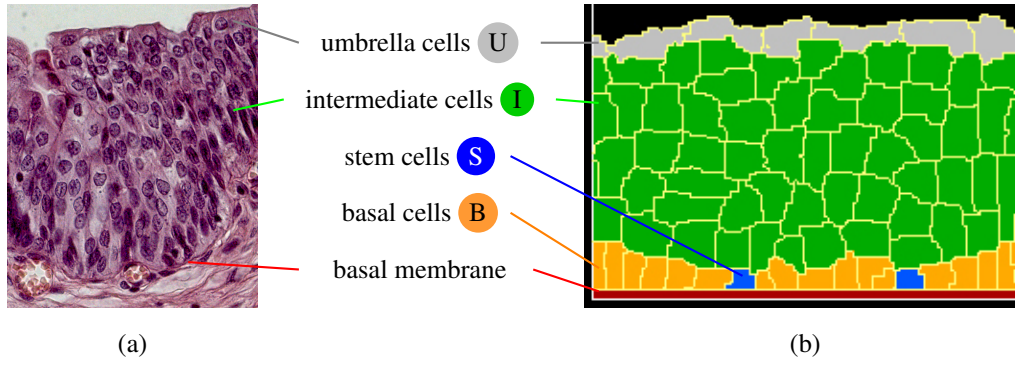
The urothelium structure shares similarities to the epidermis and is made of different layers. Both have one basal layer consisting of basal and stem cells occurring above of the basal membrane, which separates them from the deeper connective tissue. Above this are three to five layers of intermediate cells and ending with a single layer of specialized cells, which in the case of the urothelium are the umbrella cells. Fig. 1 compares a histological cut and a simplified urothelium representation. Clinical and economically relevant diseases of the urinary tract of children and adults include malformations, infections and cancer<sup>4,5</sup>.

The attributes of the urothelium are highly complex and the characteristics of each cell type of this tissue is not yet fully understood<sup>6,7</sup>. The development of precise models for further understanding of urothelial regeneration and homeostasis will be beneficial for the regenerative medicine field and cancer research<sup>6,8</sup>.

The similarity of the anatomical structure between the epidermis and the urothelium suggests the development of new models for the urothelium which are influenced by models of the epidermis. For instance, Li et al.<sup>9</sup> discuss three hypotheses for cell proliferation in epidermis: 1) asymmetric division, 2) population asymmetry and 3) population asymmetry with stem cells (PAS). We have analyzed 16 different models for cell proliferation of urothelium that simulate these hypotheses..

### 1.2 Related work

Surprisingly only few attempts to simulate the urothelium have been developed over the years to investigate and understand its proliferation. In the course of our literature search, no previous work was found that simulates the urothelium in a healthy state for the purpose of better understanding of its architecture, lineage and function. The only paper found was the simulation of Eugene Kashdan<sup>10</sup>, in which he and his colleagues simulate the urothelium as a cellular automata, inspecting the influence of matrix metalloproteinase (MMP) and secreted inhibitors from the urothelial cells to demonstrate the development of invasive



**Figure 1.** (a) Histological cut through the urothelium. (b) Simulation.

bladder cancer. Similar work to ours has been done in other types of epithelium, such as the crypts of the small intestine<sup>11</sup> and of the epidermis<sup>9</sup>. The CompuCell3D-framework<sup>12</sup> used in our paper was recently used to explore the formation of cysts in autosomal dominant polycystic kidney disease by simulating the possible effect of the activation of the gene expression of cadherin-8 in cells in a renal tubule<sup>13</sup>. In this multi-scale model it was postulated that the decrease in contact inhibition and increase of proliferation could be the cause of the activation of cadherin-8, which was then confirmed by in vitro experiments.

The urothelium models presented in this paper are extensions of the models discussed in Torelli *et al.*<sup>14</sup> and they mimic the cell proliferation in great detail: Differential adhesion between cells is used as a mechanism for cell sorting. The voiding of the bladder is also considered. Additionally, contact-inhibition and apoptosis of cells is included. The tissue can be simulated in two and three dimensions, but the focus of this paper is 2D.

The rest of the paper is structured as follows: *Results* will explain the structure of our models, the differences between these models and the reasons why these models have been chosen. It presents the findings, especially the parameters and the derived measurements and values. *Discussion* elaborates our findings in the context of the proliferation models in epidermis and other tissues. *Material and Methods* finally gives some insight into the underlying simulation techniques.

## 2 Results

The findings in this paper are based on two steps: 1) We have defined 16 models representing hypotheses of cell proliferation for the healthy tissue and 2) simulated each model with at least 25 independent runs. The simulations were then quantitatively assessed with a fitness criteria.

### 2.1 Building blocks and biological processes

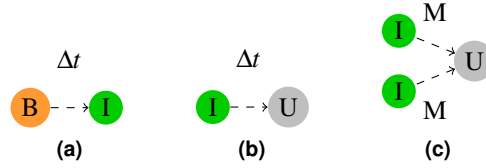
The healthy urothelium is a *flowing* tissue that is in a steady state: New cells are permanently born and older cells leave the tissue but the overall structure remains stable. Thus, our models contain birth- and death-processes which are either part of the lineage or caused by other factors.

Most of our hypotheses are based on the facts found in the textbook Campbell Walsh Urology<sup>15</sup> and other papers about the urothelium and epidermis (see below). It is generally assumed that there is enough nutrition within the tissue for the cell to thrive and proliferate if they do so according to their lineage. Nutrients diffuse from the lamina propria through the basal membrane and are consumed by adjacent cells. When cells grow and have reached their maximum (target) size they undergo mitosis or differentiate. A cell can die, either through apoptosis, or mechanically through the process of voiding. The chance of apoptosis is set differently for each cell type as listed in table 3 and ranges between  $0.1 \cdot 10^{-6}$  and  $180 \cdot 10^{-6}$  per day. Voiding of the bladder occurs every six hours. Here, apical cells that are in contact with the bladder lumen are randomly removed. The chance for being washed out is about 2% per voiding. Even a stem cell can be washed away if it reaches the surface.

### 2.2 Models

Each model shares the properties defined above and additionally consists of a combination of the various proliferation and differentiation concepts for the three cell types stem, basal and intermediate cell as shown in table 1. These concepts are the building blocks that address biological and medical questions like: Are there symmetrical or asymmetrical cell divisions? Is cell differentiation contact driven? Do intermediate cells divide or not?

First of all, to address these questions we assume that cells cannot differentiate backwards and that the path is always  $\text{S} \rightarrow \text{B} \rightarrow \text{I} \rightarrow \text{U}$  as suggested in Ho<sup>7</sup>. Additionally, we excluded time-dependent transformation (cf. 2a,b) and the special case



**Figure 2.** Possible proliferation and differentiation concepts that were excluded. A dashed line shows that a cell undergoes a direct transformation (differentiation) instead of a division, which might happen either after a certain amount of time like in a) and b) or through contact with the medium like in c). Latter one represents the special case of fusion, where two or more intermediate cells become one bigger umbrella cell to cover more surface area more quickly. This phenomenon very likely explains the findings of umbrella cells with multiple nuclei.

of fusion (cf. 2c), which is discussed in<sup>16</sup>, to concentrate on the building blocks with the highest potential for answering these questions. Table 1 shows the 16 potential division and differentiation patterns chosen for a first analysis, classified by an ID, which is used later on to identify the models. Stem and basal cells either divide and differentiate in a stem cell manner (SSD and BSD resp.) or according to the population asymmetry model in epidermis (SPA and BPA resp.). Two other hypotheses for differentiation of the basal cell are based on the differentiation into an intermediate cell when contact with the basal membrane is lost. The difference lies in the division: either with a symmetrical division into two basal cells or without any division at all (BPCD and BCD resp.). The last two hypothetical concepts were also tested for intermediate cells. The differentiation into an umbrella cell happens when the intermediate cell comes in contact with the medium (IPCD and ICD resp.).

### 2.3 Tissue developments

The models introduced in section 2.2 form 16 potential different cell lineages when combined. These cell lineages have been evaluated with computer simulations and each cell lineage model has at least  $n = 25$  different runs, i. e. runs with a different seed value for the random number generators. Some of the simulations have several hundred simulation runs. Those models were of special interest and were tested thoroughly. The initial condition for all simulations is a damaged urothelium where about 12% stem cells are randomly scattered on an otherwise empty basal membrane. This mimics the fast regeneration process of the tissue. 12% is an estimation of the number of stem cells in urothelium<sup>15</sup>.

All simulation runs of all the 16 models can be subdivided into one or more of the following tissue developments: stable, chaotic, linear and exponential overgrowing, and atrophy. A healthy tissue (Fig. 1b) recovers fairly quickly (3 to 5 days) by creating a protective layer of umbrella cells and stays stable with a single layer of basal and stem cells on the basal membrane while three to five layers of intermediate cells lie in between. This is one of the two cases of stable tissue development. The other rare case is when the stem cells randomly wander to the surface and are washed away but thanks to the proliferation of the basal and or intermediate cells, enough cells are created to keep the tissue mass in balance (Fig. 3a). A chaotic tissue development (Fig. 3b) groups those simulations with a sequence of layers different from the one of a healthy tissue. This is often the result of the combination of a random detachment of the stem cell and lack of contact differentiation of basal cells (See BSD and BPA in Table 1). When the balance between cell birth and cell death is disturbed in favor of proliferation, then the tissue overgrows. This is crucial in times of regeneration but unwanted and very dangerous in a healthy tissue, as it is the process seen in tumor development. Linear and exponential overgrowing tissue development types are shown in Fig. 3c as plots of the total number of cells taken from two simulation runs with these characteristics (SPA/BCD/ICD for the linear and SSD/BPCD/IPCD for the exponential). The opposite of tissue overgrowth is referred to as tissue atrophy or decomposition.

Simulations can be categorized as a combination of these tissue development types. For example a chaotic tissue development can also be overgrowing or atrophy. An overview of all the types of tissue development for each model is listed in Table 2. These terms were introduced as another way to describe and group the results. A more detail description of a model with a healthy and a atrophy tissue development will be described in the next section.

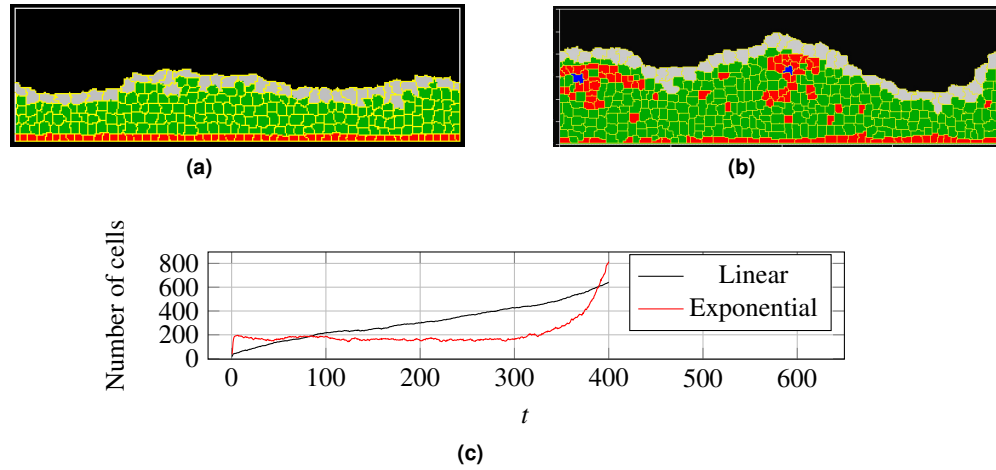
### 2.4 Fitness of the models

The computer simulations mentioned in section 2.3 were compared according to a fitness criteria (see section 4.3) calculated over the course of 720 simulated days. A fitness of 1 indicates a perfect healthy tissue whereas 0 represents a maximum disorder or a complete loss of the tissue. A summary of all the total fitness values of all the 16 models are shown in fig. 4 in form of a box and whisker plot.

Clearly, the lineage models SSD/BPCD/ICD and SPA/BPCD/ICD have the best fitness with a median fitness of 0.878 and 0.877 respectively. These two models also always develop into a healthy tissue which can be seen by the very narrow span of

Type	ID	Description	Model
Stem cells	SSD	Stem cell-like division	
	SPA	Stem cell population asymmetry	 $p_s = 0.05$ $p_a = 0.90$ $p_s = 0.05$
Basal cells	BSD	Stem cell-like division in basal cell	
	BPA	Basal cell population asymmetry	 $p_s = 0.05$ $p_a = 0.90$ $p_s = 0.05$
	BPCD	Proliferation and contact differentiation of basal cells	 $\neg \text{BM}$ and $\text{B} \dashrightarrow \text{I}$
	BCD	Only contact differentiation of basal cells	$\neg \text{BM}$ 
Intermediate cells	IPCD	Proliferation and contact differentiation of intermediate cells	 $\text{M}$ and $\text{I} \dashrightarrow \text{U}$
	ICD	Only contact differentiation of intermediate cells	$\text{M}$ 

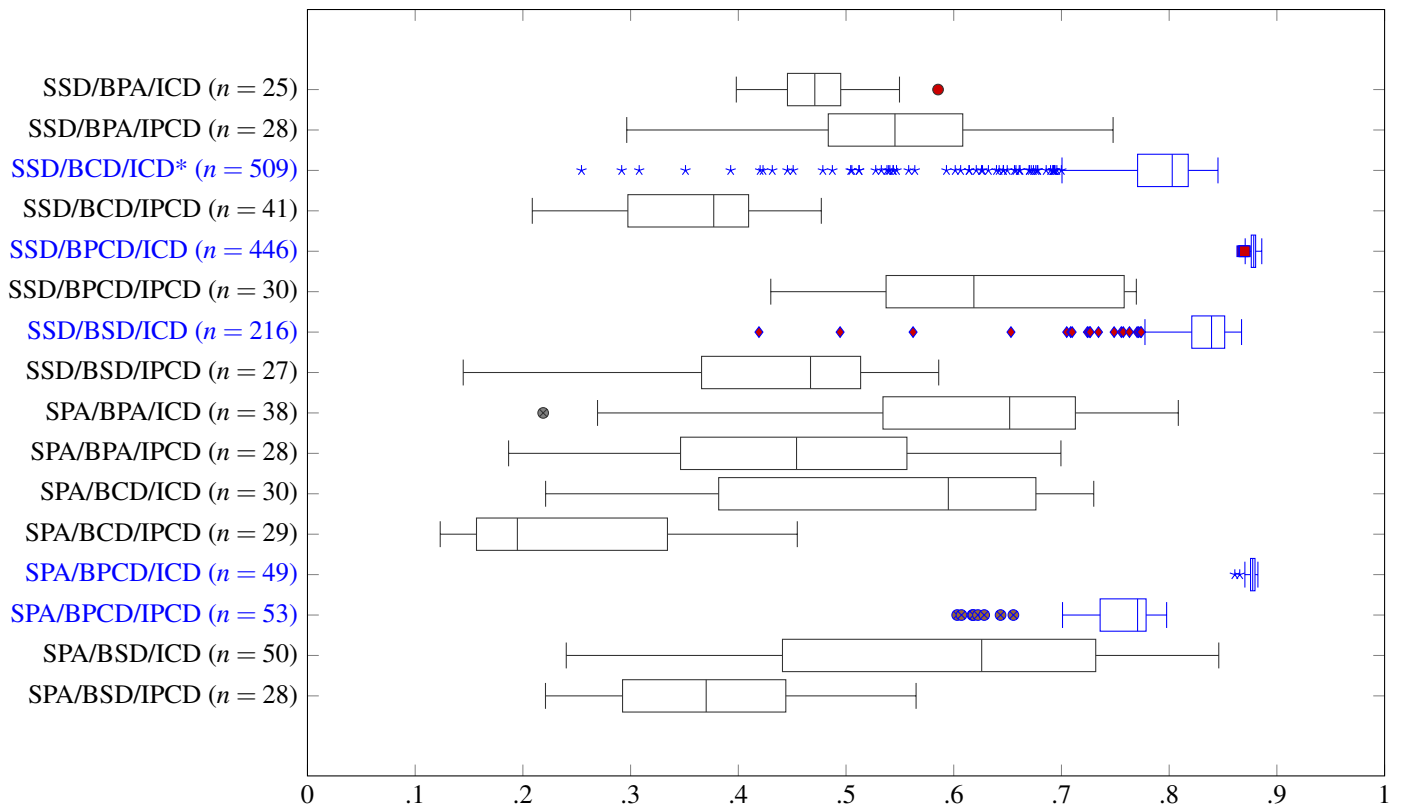
**Table 1.** Possible proliferation and differentiation concepts for the three cell types stem (S), basal (B) and intermediate (I) cell (column Type). Column ID assigns a label for a specific proliferation or differentiation rule which refers to a specific model (column Model). Per cell type group one model can be chosen. In total we have  $2 \cdot 4 \cdot 2 = 16$  lineage models. Dividing cells are expressed by a plain line and transformation (differentiation) by a dashed line. Transformation might happen either through contact (see ICD) or the loss of contact (see BCD).



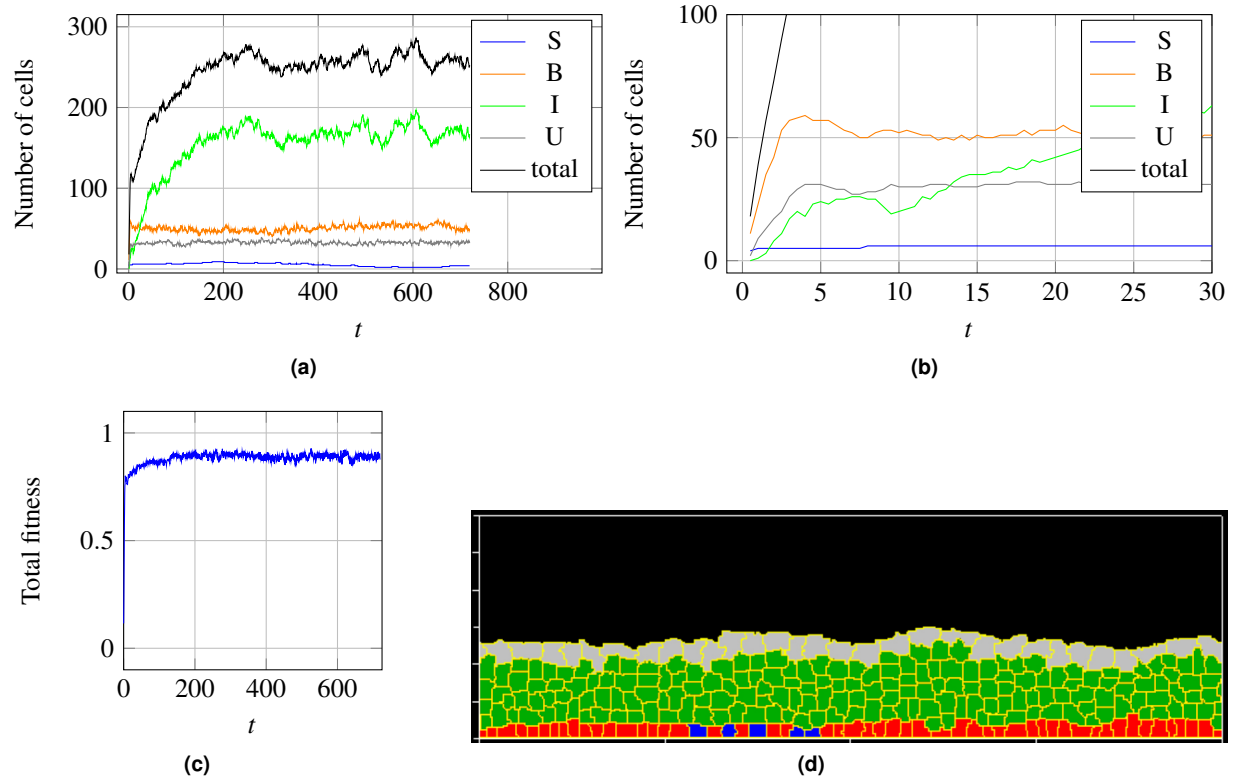
**Figure 3.** Examples of possible tissue development types. An example of a stable tissue development without stem cells taken from a SSD/BPA/ICD model is shown in a). An example of chaotic tissue development taken from a SPA/BCD/ICD model is shown in b). An example for overgrowing tissue development is not given since this would be a completely filled image without any medium (black background). Instead, the difference between linear and exponential overgrowth is shown in the form of a total cell count plot of the two. An example of atrophy tissue development is also not shown since it would be a completely black image (only medium).

Model	Stable	Chaotic	Linear growth	Exponential growth	Atrophy
SSD/BPA/ICD		•	•		
SSD/BPA/IPCD		•		•	•
SSD/BCD/ICD			•		•
SSD/BCD/IPCD				•	•
SSD/BPCD/ICD	•				
SSD/BPCD/IPCD	•			•	
SSD/BSD/ICD	•	•			
SSD/BSD/IPCD				•	•
SPA/BPA/ICD			•		•
SPA/BPA/IPCD			•		•
SPA/BCD/ICD			•		•
SPA/BCD/IPCD				•	•
SPA/BPCD/ICD	•				
SPA/BPCD/IPCD	•			•	
SPA/BSD/ICD			•		•
SPA/BSD/IPCD				•	•

**Table 2.** Occurrences of tissue development types in the different simulation runs of each model. Note that the columns can share a dependency. For instance, a tissue can develop chaotically and grow linearly.



**Figure 4.** Fitness comparison of 16 different models. The five best models are depicted in blue.  $n$ : number of simulation runs.  
\*: Contact model as published in <sup>14</sup>.

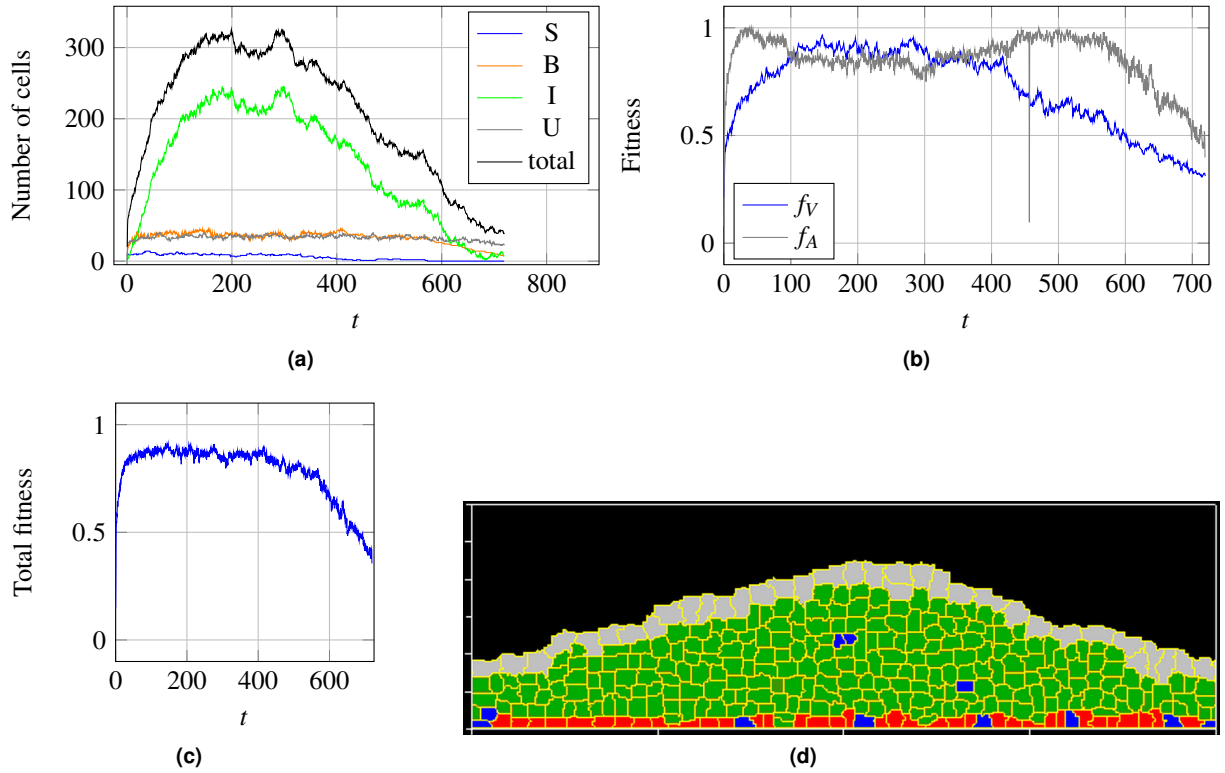


**Figure 5.** Example of a simulation run for a SPA/BPCD/ICD-model. These kind of models always create a stable, healthy tissues. The cell count from 0 to 720 days is shown in a) and from 0 to 20 days in b). After about 3 to 4 days the tissue is covered with umbrella cells (wound healing). The total fitness is shown in c) and an example for the simulated tissue at about 500 days is shown in d).

0.018 and 0.021. On the contrary the span of the lineage models SSD/BCD/ICD and SSD/BSI/ICD are much broader with 0.591 and 0.448 respectively but still perform very well having a median fitness of 0.802 and 0.839 respectively.

As an example, a simulation run with a healthy tissue development of a SPA/BPCD/ICD-model is described in more detail. Fig. 5a shows the distribution of the number of cells over a time course of 720 days. At about 200 days a steady state has been reached. This observation is similar to all other simulations of this kind. Fig. 5b shows the first 20 days. It can be seen that the tissue regenerates from just a few single stem cells in less than 5 days, which correlates to the findings from Lavelle *et al.*<sup>17</sup>. At this point in time the urothelium has formed its structure and is already covered with umbrella cells. Clearly, the number of intermediate cells still increases. Fig. 5c shows the fitness curve for this simulation run. A fit of about 85 to 88 % is reached quickly and then the structure remains stable for the rest of the time. Fig. 5d depicts a snapshot of the simulation at about 500 days. Here, a typical single layer of basal and stem cells is formed at the basal membrane followed by three to five layers of intermediate cells and finally a single layer of umbrella cells protecting all the layers beneath from the urine.

As a counter-example, a simulation run with an atrophy tissue development of a SPA/BSI/ICD-model was chosen. The total number of cells for each cell type over the course of 720 days can be seen in Fig. 6a. By day five a protective layer of umbrella cells covers the entire surface of the basal membrane and all cells in between which results in an initial high arrangement fitness close to 1 (see Fig. 6b). It continues to grow in a linear manner for 150 days growing stronger where more stem cells lie underneath forming a hill in the middle as can be seen in Fig. 6c. This effect makes the arrangement fitness decline slightly because the number of intermediate cell layers should not be more than five or less than three. The tissue mass stays stable for approximately another 200 days maintaining 6 to 14 stem cells from day one. By being a model with stem cell population asymmetry the number of stem cells can vary greatly which only depends on pure chance. After the first year there is a decline in the number of stem cells which affects the entire tissue mass. This is also been reflected in both total number of cells (Fig. 6a) and the volume fitness (Fig. 6b) and therefore also the total fitness (Fig. 6d). At day 573 the last stem cells divides symmetrically into two basal cells. Without a source of proliferation the tissue will continue to fade away until no cell would remain. This would have been the case if the simulation had continued past the 720 days.



**Figure 6.** Example of a simulation run for a SPA/BSD/ICD-model. These models are intrinsically unstable. The cell count over the entire 720 days is shown in a). The volume ( $f_V$ ) and arrangement fitness ( $f_A$ ) is shown in b) and the total fitness in c) (see section 4.3). At day 573 no more stem cells are present in the tissue, which will result in total atrophy. An example for the simulated tissue at about 200 days is shown in d).



Model	parameters								measured				
	growth rate (%/d)				apoptosis chance (10 <sup>-6</sup> /d)				cycle or life time (h)				healing (d)
	S	B	I	U	S	B	I	U	S	B	I	U	
SSD/BCD/ICD	15	13	11	10	0	0.1	1	2	73 ± 0.9	640 ± 66	1320 ± 400	582 ± 30	< 30
SSD/BPCD/ICD	12	12	10	10	0	2	2	4	289 ± 4.5	155 ± 1.4	879 ± 39	415 ± 19	< 6
SSD/BSI/ICD	11	10	9	8	0	20	20	40	281 ± 6.3	272 ± 4.0	907 ± 171.7	414 ± 16.1	< 6
SPA/BPCD/ICD	12	11	10	90	0	2	2	4	287 ± 9.7	156 ± 4.1	920 ± 44	424 ± 9.6	< 6
SPA/BPSD/IPCD	12	11	10	9	0	20	150	180	273 ± 8.8	138 ± 5.3	87 ± 7.3	187 ± 4.5	< 6

**Table 3.** Parameters and derived data for the five best of the 16 models according the fitness function (cf. 4). The left part shows the parameters for all cell types (S, B, I, and U) used to obtain a healthy tissue. The growth rate is in percent of the regular maximal cell volume  $V_{max}$  (in  $\mu\text{m}^3$ ) per day when cells are contact-inhibited. The apoptosis chance is the likelihood in  $10^{-6}$  per day that a cells undergoes apoptosis. The right part *measured* shows the derived data: cycle or life times is the average time that a cells of a specific cell type life before their undergo mitosis, differentiate or die. Healing shows the time until the urothelium is covered completely with umbrella cells when starting with an empty basal membrane and some stem cells (wound healing scenario).

## 2.5 Adjusted parameters and derived measurements

Each model comes with a set of parameters which refine the building blocks and the general mechanisms. Here we describe those parameters that are unknown and adjusted to fit the models in the previous section. The remaining parameters are elaborated in section 4.2. Table 3 shows the parameters which are varying from model to model. The building blocks SPA and BPA always have a likelihood of  $p_s = 0.05$  for symmetrical and  $p_a = 0.9$  for asymmetrical divisions. These numbers differ from those suggested in the epidermis model<sup>9</sup> where  $p_s = 0.1$  and  $p_a = 0.8$ . If the chance for a symmetrical division in the urothelium was set to 0.1 the tissue very frequently lost all of its stem cells.

## 3 Discussion

### 3.1 Cell divisions in intermediate cells

The adult urothelium of the bladder is a stratified epithelium with three cell layers and cell types (basal-, intermediate-, and superficial or umbrella cells) similar to the skin epithelium. Therefore traditional hypothesis of regeneration and differentiation suggests that a progenitor cell population is located in the basal cell layer and gives rise to all layers of urothelium and regenerates the mucosa in case of mucosal injury<sup>7,18</sup>. In contrast, other studies propose that intermediate cells can self-renew and generate superficial daughter cells, indicating an alternative pool of adult urothelial progenitors<sup>6</sup>. Also, it was shown that intermediate cells are highly proliferative and show rapid cell regeneration in response to injury or infection<sup>19</sup>.

However, our findings clearly show an advantage of models with a small proportion of basal cells with stem cell division located at the basal membrane (SSD/BPCD/ICD and SPA/BPCD/ICD) in comparison to models with intermediate cell divisions. Interestingly, the SSD/BCD/ICD model, where basal cells do not divide, is also able to create a healthy tissue. But this model fails when wound healing is considered as the regeneration time is about 30 days. The remaining four models all show a realistic wound healing time between 3 to 6 days as supported by the literature<sup>20</sup>. Three of the four remaining models in table 3 all have similar cycle times. Solely SPA/BPCD/IPCD also has proliferating intermediate cells but a slightly worse fitness (see 4). It is an open question whether this model could obtain a better fitness if its parameters would be better adjusted. Also, it is worth mentioning that according to the two best models it does not matter whether stem cells separate in a stem cell-like manner (SSD/PBCD/ICD) or according to the population asymmetry theory (SPA/PBCD/ICD).

Experimental data supports the finding that urothelial stem cells reside in the basal cell layer, because proliferation is observed in the lower cell layers. This was shown using label retention studies<sup>21,22</sup>. Further data by Gaisa et al.<sup>23</sup> sought to locate the stem cell niche in the human urothelium by demonstrating expansion from a single mutated stem cell by using naturally occurring mitochondrial DNA (mtDNA) mutations as a marker of clonal expansion. These data clearly showed based on histology that the human adult urothelium is maintained by stem cell-derived clonal fields of progeny.

### 3.2 Adhesion to the basal membrane

Tissue homeostasis under “healthy conditions” needs coordination of cell proliferation, migration and differentiation which are interrupted during carcinogenesis. The main finding of this study is the high intrinsic stability of healthy tissue when a cell contact to the basal membrane and medium was supposed. The best two models (SSD/BPCD/ICD and SPA/BCPD/ICD) use contact differentiation as a control mechanism. Even the SSD/BSD/ICD model that only uses differential adhesion for cell sorting can achieve an acceptable fitness.

The normal urothelium expresses several adhesion molecules implicated in cell-cell and cell-matrix interactions, including E; P-cadherin, CD44 and several integrins<sup>24,25</sup>. These molecules are central for cell polarity and localization. Cadherins are transmembrane glycoproteins central for cell-cell and together with integrins for cell-matrix interactions<sup>26</sup>. It was shown that membranous P-cadherin expression was confined to the basal layer of normal urothelium<sup>25</sup>. Deregulation of these molecules, the “cadherine switch”, is clearly linked to tumor invasiveness in various epithelial malignancies and bladder cancer<sup>27</sup>. Integrins are cell adhesion receptors that bind to extracellular matrix ligands, cell-surface ligands or soluble ligands. They are important for cell attachment and control cell migration, cell cycle progression and programmed cell death<sup>28,29</sup>. Again alteration of these molecules are linked to tumor progression in bladder cancer<sup>30</sup>.

The association of alterations in cell adhesion molecules with bladder cancer progression and invasion underline the importance of cell adhesion for normal patterns of urothelial tissue formation and homeostasis. This furthermore suggests further options using the proposed computational model identifying mechanisms by which an “altered cell population” may give rise to invasive tumors, which is essential to the understanding of the origin and biology of bladder cancer.

### 3.3 Conclusion

Our work evaluates for the first time several models of cell division and differentiation using a multi-scale approach with CompuCell3D<sup>12</sup>. These simulations consider the complexity of cell characteristics and differentiation in regeneration of the adult urothelium after injury.

## 4 Material and methods

### 4.1 Modelling techniques

The CompuCell3D framework<sup>12</sup> was utilized and extended with Python scripts. CompuCell3D is based on the Glazier-Graner-Hogeweg (GGH) approach<sup>31</sup> that is also known as the Cellular Potts Model (CPM). GGH models are Monte Carlo simulations with agent-based extensions. A biological cell is represented as a cohesive cluster of pixels (or voxels) placed on a two or three dimensional lattice. The time advances in discrete steps. Each step is called a Monte-Carlo-Step (MCS).

The core of any GGH model is the effective energy  $E$  that is minimized in the course of the simulation, reflecting the physical law to minimize the energy of a system. The composition of  $E$  describes the cell behaviors and interactions in a physical and biological manner – in our simulations  $E$  consists of the following components:

$$E = E_V + E_S + \lambda_A E_A \quad (1)$$




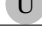
$E_V$  is a term that describes the energy for the cell's volumes,  $E_S$  for the cell's surface and  $E_A$  considers the adhesion of two cell's surfaces.  $E_V$  is the sum of the volume deviations as squared error for each cell ( $\sigma$  according to the notation in<sup>12</sup>). Each cell occupies a certain volume in the current state ( $V_a(\sigma)$ ) and has a target volume ( $V_t(\sigma)$ ), which is the volume a cell should reach to be healthy and varies depending on the cell type. Any deviation to the target volume increases the energy  $E_V$  as follows:  $E_V = \sum [\lambda_V(\sigma)(V_a(\sigma) - V_t(\sigma))^2]$ . The parameter  $\lambda_V(\sigma)$  is cell type dependent and can be seen as an inverse compressibility factor, with lower values increasing fluctuations of a cell's volume about its target volume. The energy  $E_S$  is implemented in similar fashion but instead of the volume,  $E_S$  takes the surface of each cell into account and weights the surface energy with  $\lambda_S(\sigma)$ . For the term  $E_A$  please refer to Swat *et al.*<sup>12</sup>.  $\lambda_V$ ,  $\lambda_S$  and  $\lambda_A$  are weights that allows us to adjust the importance for each energy term. For instance, as cells are not compressible they must maintain their volume but can have flexible surface. This is achieved by setting  $\lambda_V > \lambda_S$ .

### 4.2 Configuration







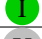

This section describes biological constants which could be determined and parameters, in particular those which are required for GGH simulations.

#### 4.2.1 Space and time

The space in which all the simulations run is 800  $\mu\text{m}$  in width and 150  $\mu\text{m}$  in height. We used a pixel density of 0.8 pixel /  $\mu\text{m}$  which leads to a lattice of  $640 \times 120 \times 1$  pixels. Note that the  $z$ -dimension is always 1 pixel to get 2D plane. The boundary conditions for the  $x$ -axis is set to periodical, while the  $y$ - and  $z$ -axes are fixed. Periodical in this case means that the left and right boundary are connected. The time resolution is 500 MCS per day and the urothelium was simulated for about two years (720 days) which is equivalent to a total of 360,000 MCS.

Cell type		$V_{min}$	$d_{min}$	$V_{max}$	$d_{max}$	Volume	Surface
Stem		268	8	523	10	perfect	average
Basal		381	9	523	10	important	average
Intermediate		905	12	1767	15	important	poor
Umbrella		1767	15	3591	19	important	poor

**Table 4.** Cell properties. Volumes  $V$  in  $\mu\text{m}^3$ , diameters  $d$  in  $\mu\text{m}$ . Columns *Volume* and *Surface* are adjusted with the weights  $\lambda_V$  and  $\lambda_A$ , respectively.

Types		M	BM				
Medium	M	0	14	14	14	14	4
Basal membrane	BM		-1	1	3	12	12
Stem cell				6	4	8	14
Basal cell					5	8	12
Intermediate cell						6	4
Umbrella cell							2

**Table 5.** Surface tension values for the four cell types, the basal membrane (BM) and the medium (M). The values are according to CompuCell3D conventions: small values represent high adhesion, higher values less adhesion/greater repulsion.

#### 4.2.2 Cell properties

Tables 4 and 5 list the remaining cell properties of the four cell types that were not already introduced as parameters. These are the minimum and maximum volumes and diameters as well as how rigorously a cell type should adhere to these volume and surface restrictions. The data was obtained by analyzing histological cuts<sup>15,32–36</sup>. We assume, by default, that cells have a circular or spherical shape. However, as cells are squeezed in a dense tissue, their shape is different. The more strict a cell type has to follow the surface restrictions, the stiffer a cell becomes. Stiffness limits the cell movement and it can be controlled by  $\lambda$  factor in eq. 1.

Contact inhibition is a well-known property of normal cells and contributes to the regulation of proper tissue growth, differentiation, and development. Contact inhibition of proliferation was included whereas contact inhibition of locomotion was not considered in this work. Former was postulated due to the fast healing times in contrast to the long turnover rates of the healthy tissue<sup>1</sup>. The cell proliferation rate in our simulations is accelerated by a factor of 50 when cells are not completely surrounded by other cells.

Finally, our models incorporate a cell sorting mechanism as the simulations by Torelli *et al.*<sup>14</sup> have shown that a correct layout of the cell layers can hardly be achieved without sorting. Cell sorting is achieved according to the differential adhesion hypothesis. It claims that cells move while minimizing the energy when cell membranes with specific adhesion molecules interact<sup>37</sup>. The combinations of all four cell types, the basal membrane and the medium results in 21 different surface tension values that are listed in table 5. The energies are set in a way that free floating cells would form an onion ring like structure with the basal membrane in the center, followed by stem and basal cells, then intermediate cells and on the surface umbrella cells. These adhesion energies were fixed in all simulations.

### 4.3 Fitness function

In the following section we assume that we can measure the arrangement of cells and their volumes at specific points in time. Any simulation starts at time  $t_0 = 0$  and ends at time  $t_e$ , typically  $t_e = 720$  d. In between this range we can sample the tissue at time points  $t_0, t_1, \dots, t_e$ . For simplicity, in the following definitions  $t_i$  is omitted. We write  $f = f(t_i)$ .

#### 4.3.1 Arrangement fitness function

The arrangement fitness function  $f_A$  surveys to ensure that the cell strata are in the correct order. This is done by a function applying Boolean terms. It reaches an optimum of 1 if the urothelium reaches a state where the basal and stem cells layer is right above the basal membrane, followed by the various layers of intermediate cells and finally with one layer of umbrella cells, before the medium occupies the intraluminal space. In the worst case scenario, 0, the simulation does not create any cells. This equation is defined as followed:

$$f_a^* = \begin{cases} \frac{1}{(1-L_B)+(lib-L_I)+(1-L_U)+1} & \text{if number of layers} > 0 \\ 0 & \text{otherwise.} \end{cases}$$

$L_B = 1$  if the first layer is made of cell type basal or stem otherwise 0.  $L_U = 1$  if the last layer is made of cell type umbrella otherwise 0.  $lib$  (layers in between) is the number of strata in between the first and last layer.  $L_I$  is the number of layers made of intermediate cells.  $lib - L_I$  results in the number of cells wandering away from their intended layer.

The function  $f_A^*$  is then calculated column-wise for every  $25\mu\text{m}$  of the tissue resulting in a total of 31 samples. Out of these values, the average is taken and assigned to  $f_A$ .

#### 4.3.2 Volume fitness function

Since no information was found in the literature search regarding the volume of each of the urothelial cell types, the relative volumes  $v_{B,S}, v_I, v_U$  values were calculated as an average from a variety of histological pictures of the urothelium in a relaxed state (empty bladder) that were found in urology text books<sup>15,32–36</sup>. The results are  $v_{B,S} = 10\%$ ,  $v_I = 67\%$ ,  $v_U = 23\%$  of an averaged urothelium thickness of  $85\mu\text{m}$ . With these values a non linear volume fitness function  $f_V$  was created and is described as followed:

$$f_{V_i} = \frac{1}{4 \left( \frac{V_{S_i} - V_{I_i}}{V_{S_i}} \right)^2 + 1}$$

$V_S$  and  $V_I$  is the desired (should) and actual (is) volume of all cells of a specific type  $i$ .  $V_S$  is equivalent to the width times the depth of the simulated urothelium times a height of  $85\mu\text{m}$ . The overall fitness volume function  $f_V$  is the arithmetic mean for all urothelium cell types (S,B), I, and U where S and B are considered as the group of cells laying on the basal membrane.

#### 4.3.3 Total fitness

The total fitness function for a specific point  $t_i$  averages the arrangement and volume fitness:

$$f(t_i) = \frac{f_v(t_i) + f_a(t_i)}{2}$$

The total fitness as applied in fig. 4 is the average total fitness value for all points in time:

$$f = \frac{1}{e+1} \sum_{i=0}^e f(t_i)$$

with  $e+1$  indicating the number of time points.

#### 4.4 Software

The Python scripts for CompuCell3D are hosted as an open source project at Github (<https://github.com/informatik-mannheim/Moduro-CC3D>) with the name Moduro-CC3D. The simulation runs are analyzed with the Moduro toolbox that is also available at Github (see <https://github.com/informatik-mannheim/Moduro-Toolbox>).

#### References

1. Khandelwal, P., Abraham, S. N. & Apodaca, G. Cell biology and physiology of the uroepithelium. *Am J Physiol Ren. Physiol* F1477–F1501 (2009).
2. Hicks, R. The mammalian urinary bladder: an accommodating organ. *Biol Rev Camb Philos Soc.* **50**, 215–46. (1975).
3. Jost, S. Cell cycle of normal bladder urothelium in developing and adult mice. *Virchows Arch B Cell Pathol Incl Mol Pathol.* **57**, 27–36 (1989).
4. Jemal, A. *et al.* Global cancer statistics (March, April / 2011). URL <http://cacancerjournal.org>.
5. Atala, A., Bauer, S., S, S. S., Yoo, J. & Retik, A. Tissue-engineered autologous bladders for patients needing cystoplasty. *Lancet* **15**, 1241–6. (2006).
6. Yamany, T., van Batavia, J. & Mendelsohn, C. Formation and regeneration of the urothelium. *Curr Opin Organ Transpl.* **19**, 323–330 (2014). URL <http://dx.doi.org/10.1097/MOT.0000000000000084>.
7. Ho, P. L., Kurtova, A. & Chan, K. S. Normal and neoplastic urothelial stem cells: getting to the root of the problem. *Nat. reviews. Urol.* **9**, 583–594 (2012). URL <http://dx.doi.org/10.1038/nrurol.2012.142>.

8. Osborn, S. L. *et al.* Induction of human embryonic and induced pluripotent stem cells into urothelium. *Stem cells translational medicine* **3**, 610–619 (2014). DOI 10.5966/sctm.2013-0131.
9. Li, X. *et al.* Skin stem cell hypotheses and long term clone survival – explored using agent-based modelling. *Sci. Rep.* **3**, 1904 (2013). URL <http://dx.doi.org/10.1038/srep01904>.
10. Kashdan, E. Hybrid discrete-continuous model of invasive bladder cancer. *Math. Biosci. Eng.* **Vol. 10**, 729–742 (2013).
11. Buske, P. *et al.* A comprehensive model of the spatio-temporal stem cell and tissue organisation in the intestinal crypt. *PLoS Comput. Biol* **7** (2011). URL <http://dx.doi.org/10.1371/journal.pcbi.1001045>.
12. Swat, M. H. *et al.* Multi-scale modeling of tissues using compucell3d. *Comput. Methods Cell Biol.* 325–366 (2012). URL <http://dx.doi.org/10.1016/B978-0-12-388403-9.00013-8>.
13. Belmonte, J. M. *et al.* Virtual-tissue computer simulations define the roles of cell adhesion and proliferation in the onset of kidney cystic disease. *Mol. Biol. Cell* **27**, 3673–3685 (2016). URL <http://dx.doi.org/10.1091/mbc.E16-01-0059>.
14. Torelli, A., Siegel, F., Erben, P. & Gumbel, M. Modeling of the urothelium with an agent based approach. In *Bioinformatics and Biomedical Engineering*, vol. 9044, 375–385 (Springer, 2015). URL [http://dx.doi.org/10.1007/978-3-319-16480-9\\_37](http://dx.doi.org/10.1007/978-3-319-16480-9_37).
15. Wein, A. J., Kavoussi, L. R., Campbell, M. F. & Walsh, P. C. *Campbell-Walsh urology* (Elsevier Saunders, Philadelphia and PA, 2012), 10th ed. edn. URL <http://www.worldcat.org/oclc/747952227>.
16. HICKS, R. M. THE MAMMALIAN URINARY BLADDER AN ACCOMMODATING ORGAN. *Biol. Rev.* **50**, 215–246 (1975). URL <http://dx.doi.org/10.1111/j.1469-185x.1975.tb01057.x>.
17. Lavelle, J. *et al.* Bladder permeability barrier: recovery from selective injury of surface epithelial cells. *Am. journal physiology. Ren. physiology* **283**, F242–F253 (2002). DOI 10.1152/ajprenal.00307.2001.
18. Shin, K. *et al.* Hedgehog/wnt feedback supports regenerative proliferation of epithelial stem cells in bladder. *Nat.* **472**, 110–114 (2011). URL <https://doi.org/10.1038/nature09851>. DOI 10.1038/nature09851.
19. Osborn, S. L. & Kurzrock, E. A. Production of urothelium from pluripotent stem cells for regenerative applications. *Curr. Urol. Reports* **16** (2014). URL <https://doi.org/10.1007/s11934-014-0466-6>. DOI 10.1007/s11934-014-0466-6.
20. Gandhi, D. *et al.* Retinoid signaling in progenitors controls specification and regeneration of the urothelium. *Dev. Cell* **26**, 469–482 (2013). URL <https://doi.org/10.1016/j.devcel.2013.07.017>. DOI 10.1016/j.devcel.2013.07.017.
21. Kurzrock, E. A., Lieu, D. K., deGraffenried, L. A., Chan, C. W. & Isseroff, R. R. Label-retaining cells of the bladder: candidate urothelial stem cells. *AJP: Ren. Physiol.* **294**, F1415–F1421 (2008). URL <https://doi.org/10.1152/ajprenal.00533.2007>. DOI 10.1152/ajprenal.00533.2007.
22. Zhang, H. *et al.* Label retaining and stem cell marker expression in the developing rat urinary bladder. *Urol.* **79**, 746.e1–746.e6 (2012). URL <https://doi.org/10.1016/j.urology.2011.10.051>. DOI 10.1016/j.urology.2011.10.051.
23. Gaisa, N. T. *et al.* The human urothelium consists of multiple clonal units, each maintained by a stem cell. *The J. Pathol.* **225**, 163–171 (2011). URL <https://doi.org/10.1002/path.2945>. DOI 10.1002/path.2945.
24. Southgate, J., Hutton, K. A., Thomas, D. F. & Trejdosiewicz, L. K. Normal human urothelial cells in vitro: proliferation and induction of stratification. *Lab. investigation; a journal technical methods pathology* **71**, 583–594 (1994).
25. Rieger-Christ, K. M. *et al.* Expression of classic cadherins type i in urothelial neoplastic progression. *Hum. pathology* **32**, 18–23 (2001). DOI 10.1053/hupa.2001.21140.
26. Weber, G. F., Bjerke, M. A. & DeSimone, D. W. Integrins and cadherins join forces to form adhesive networks. *J. cell science* **124**, 1183–1193 (2011). DOI 10.1242/jcs.064618.
27. Bryan, R. T. & Tselepis, C. Cadherin switching and bladder cancer. *The J. urology* **184**, 423–431 (2010). DOI 10.1016/j.juro.2010.04.016.
28. Humphries, M. J. Integrin structure. *Biochem. Soc. transactions* **28**, 311–339 (2000).
29. Takada, Y., Ye, X. & Simon, S. The integrins. *Genome biology* **8**, 215 (2007). DOI 10.1186/gb-2007-8-5-215.
30. Behnsawy, H. M. *et al.* Expression of integrin proteins in non-muscle-invasive bladder cancer: significance of intravesical recurrence after transurethral resection. *BJU international* **107**, 240–246 (2011). DOI 10.1111/j.1464-410X.2010.09534.x.

31. Balter, A., Merks, R. M. H., Popławski, N. J., Swat, M. & Glazier, J. A. The glazier-graner-hogeweg model: Extensions, future directions, and opportunities for further study. In *Single-Cell-Based Models in Biology and Medicine*, 151–167 (Birkhaeuser Basel, 2007). URL [http://dx.doi.org/10.1007/978-3-7643-8123-3\\_7](http://dx.doi.org/10.1007/978-3-7643-8123-3_7).
32. Gasser, T. *Basiswissen Urologie*. Springer-Lehrbuch (Springer-Verlag Berlin Heidelberg, Berlin and Heidelberg, 2011), 5 edn.
33. Rübben, H. (ed.) *Uroonkologie* (Springer Berlin, Berlin, 2013), 6., aufl. 2013 edn.
34. Hautmann, R. & Huland, H. *Urologie: Mit 176 Tabellen*. Springer-Lehrbuch (Springer, Heidelberg, 2010), 4 edn.
35. Hallscheidt, P. & Haferkamp, A. *Urogenitale bildgebung* (Springer, Berlin, 2010).
36. Schultz-Lampel, D., Goepel, M. & Haferkamp, A. *Urodynamik*. SpringerLink : Bücher (Springer Berlin Heidelberg, Berlin and Heidelberg, 2012), 3 edn.
37. Glazier & Graner. Simulation of the differential adhesion driven rearrangement of biological cells. *Phys. review. E, Stat. physics, plasmas, fluids, related interdisciplinary topics* **47**, 2128–2154 (1993).

### **Acknowledgments**

We would like to thank Thomas Ihme for his CUDA server and Mathuraa Pathmanathan for the first version of the Moduro toolbox.

### **Contributions**

A.T. designed models, performed simulations, developed analytic tools, analyzed data and wrote the paper; P.E. wrote the paper; J.D. designed models and performed simulations; M.G. designed models, developed analytic tools and wrote the paper.

### **Additional information**

Competing financial interests: The authors declare no competing financial interests.